Evaluation of ^{13}C isotopic tracers for metabolic flux analysis in mammalian cells

Christian M. Metallo[*], **Jason L. Walther**[*], and **Gregory Stephanopoulos**[†]

Department of Chemical Engineering, Massachusetts Institute of Technology, Building 56 Room 469C, 77 Massachusetts Ave, Cambridge, MA 02139; telephone: 617-253-4583; fax: 617-253-3122; e-mail: gregstep@mit.edu

Abstract

[13]C metabolic flux analysis (MFA) is the most comprehensive means of characterizing cellular metabolic states. Uniquely labeled isotopic tracers enable more focused analyses to probe specific reactions within the network. As a result, the choice of tracer largely determines the precision with which one can estimate metabolic fluxes, especially in complex mammalian systems that require multiple substrates. Here we have experimentally determined metabolic fluxes in a tumor cell line, successfully recapitulating the hallmarks of cancer cell metabolism. Using these data, we computationally evaluated specifically labeled ^{13}C glucose and glutamine tracers for their ability to precisely and accurately estimate fluxes in central carbon metabolism. These methods enabled us to to identify the optimal tracer for analyzing individual fluxes, specific pathways, and central carbon metabolism as a whole. $[1,2-^{13}C_2]$glucose provided the most precise estimates for glycolysis, the pentose phosphate pathway, and the overall network. Tracers such as $[2-^{13}C]$glucose and $[3-^{13}C]$glucose also outperformed the more commonly used $[1-^{13}C]$glucose. $[U-^{13}C_5]$glutamine emerged as the preferred isotopic tracer for analysis of the tricarboxylic acid (TCA) cycle. These results provide valuable, quantitative information on the performance of ^{13}C-labeled substrates and can aid in the design of more informative MFA experiments in mammalian cell culture.

Keywords

Metabolic flux analysis; confidence intervals; isotopic tracers; tumor cells

Introduction

[13]C metabolic flux analysis (MFA) is an effective tool for characterizing the metabolic phenotype of organisms at the systems level. This technique has been described extensively in the literature and typically involves the application of a labeled substrate to a biological system, measurement of label incorporation within metabolite pools, and computational estimation of intracellular fluxes that fit the observed data (Sauer, 2006, Tang et al., 2009b). The acquisition of systemwide information on cellular metabolism enables identification of

novel therapeutic targets for disease (Munger et al., 2008), provides information on substrate utilization within specific metabolic pathways (Kharroubi et al., 1992, Neese et al., 1993), and offers insight into key reactions of product synthesis (Kleijn et al., 2007, Antoniewicz et al., 2007b). Regardless of the specific application, MFA must generate precise and accurate flux data to effectively differentiate between cellular phenotypes (Tang et al., 2009a).

The choice of tracer dictates the mass isotopomer distribution (MID) of each metabolite for a given set of fluxes. The sensitivity of the MIDs, in turn, to changes in the pathway fluxes ultimately determines the confidence of flux estimates, which are as important as the flux values themselves (Antoniewicz et al., 2006). Stationary MFA is conducted when the labeled substrate is at isotopic steady state and does not utilize pool size or transient data; as such, this technique is especially reliant upon the specific tracer used. Depending on the particular bioreaction network, nonstationary MFA may be preferable and can also benefit from a informed choice of tracer (Noh and Wiechert, 2006, Noh et al., 2006). The issue of tracer choice is more complex in mammalian cell systems that utilize multiple carbon sources (e.g., glucose and glutamine) and are grown in complex media. To probe specific pathways, researchers have applied a wide array of isotopically labeled substrates, including glucose, glutamine, or atypical substrates such as propionate or succinate (Burgess et al., 2007, Yang et al., 2008, Yoo et al., 2008). For example, $[1,2\text{-}^{13}C_2]$glucose is commonly employed for analysis of the pentose phosphate pathway (PPP) (Boros et al., 2005), whereas $[3\text{-}^{13}C]$glucose or $[3\text{-}^{14}C]$glucose provide information on pyruvate oxidation (Holleran et al., 1997, Munger et al., 2008). Many tracers effectively label metabolites in the tricarboxylic acid (TCA) cycle, but the presence of anaplerotic reactions and glutamine incorporation (through glutaminolysis or reductive carboxylation) make it difficult to identify the optimal tracer for measuring all net and exchange fluxes within the network.

Systems biology concerns itself with the acquisition, integration, and analysis of complex data sets. MFA was one of the first manifestations of systems-level analysis in complex, biological systems and is unique among systems biology tools in that it allows determination of actual enzyme function (i.e., fluxes) (Stephanopoulos and Vallino, 1991, Nielsen, 2003, Hellerstein, 2004). Unlike concentration-based methodologies, MFA requires both experimental measurement and computational models to elucidate these time-dependent parameters (Sauer, 2006). As such, experimental design to maximize meaningful information is crucial in MFA and requires model-based interpretation. Researchers have recently described methods to optimize measurement sets for flux determination (Rantanen et al., 2006, Chang et al., 2008); however, the choice of tracer is an equally important parameter. Because the tracer strongly influences flux estimation quality and can usually be chosen from a wide array of available isotopic substrates, judicious tracer selection is a major component of this experimental design process. As a result, a systematic analysis of available ^{13}C-labeled tracers and associated confidence intervals (i.e., sensitivities) for each estimated flux is warranted. Optimization of tracer choice will enable researchers to more precisely measure specific fluxes in high-throughput applications that aim to screen the metabolic effects of drugs in cells (Borner et al., 2007, Sekhon et al., 2008).

Some initial investigation has occurred in this area. Sriram and colleagues have conducted a Monte Carlo-based analysis of experimental precisions (using standard deviations) when using different combinations of $[U\text{-}^{13}C_6]$glucose, $[1\text{-}^{13}C]$glucose, and naturally labeled glucose in a mammalian network (Sriram et al., 2008). Similar studies have been performed in microbial systems, which typically consume a single carbon source (Noh et al., 2006). However, a detailed investigation of confidence intervals generated from different, unique tracers in a two-substrate network has never been completed.

Here we have experimentally determined the flux network in a carcinoma cell line and used these data to calculate the confidence intervals for each flux when using different ^{13}C-labeled glucose and glutamine tracers. An elementary metabolite unit (EMU)-based method was used to rapidly estimate flux profiles and confidence intervals from simulated measurements in stationary MFA experiments (Antoniewicz et al., 2007a, Young et al., 2008). We were able to quantitatively validate the effectiveness of specific ^{13}C tracers in a cancer cell network and identify the best choice for analysis of individual reactions and pathways. A scoring algorithm was employed to determine the optimal tracer for the overall model and for subnetworks representing glycolysis, the PPP, and the tricarboxylic acid (TCA) cycle. These results may significantly improve the efficiency of MFA experiments in high-throughput applications and clinical samples where biological material is limited (Boros et al., 2003).

Materials and Methods

Cell culture and metabolite extraction

The A549 lung carcinoma cell line was obtained from ATCC and maintained in high-glucose DMEM supplemented with 4 mM glutamine, 10% FBS, and 100 U ml^{-1} penicillin/streptomycin (Invitrogen). For labeling experiments, semi-confluent cells in a 10-cm dish were cultured in glucose-free DMEM (Sigma) with the above supplements and a 25mM 1:1 mixture of [U-^{13}C$_6$]glucose and [1-^{13}C]glucose (Cambridge Isotope Laboratories) for 6 hours to achieve isotopic steady state. Spent medium was collected and analyzed for glucose, lactate, and glutamine consumption on a YSI7100 analyzer. Cells were quenched with 1 ml ice cold methanol, an equal volume of water was added, and cells were collected with a cell scraper. Four volumes of chloroform were added, and the cells were vortexed and held on ice for 30 minutes for deproteinization. After addition of 2 ml water, samples were centrifuged at 3000 *g* for 20 minutes at 4°C. The aqueous phase was collected in a new tube and evaporated under airflow at room temperature.

Derivatization and GC/MS measurements

Dried polar metabolites were dissolved in 60 µl of 2% methoxyamine hydrochloride in pyridine (Pierce), sonicated for 30 minutes, and held at 37°C for 2 hours. After dissolution and reaction, 90 µl MBTSTFA + 1% TBDMCS (Pierce) was added and samples were incubated at 55°C for 60 minutes. Gas chromatography/mass spectrometry (GC/MS) analysis was performed using an Agilent 6890 GC equipped with a 30m DB-35MS capillary column connected to an Agilent 5975B MS operating under electron impact (EI) ionization at 70 eV. One µl of sample was injected in splitless mode at 270°C, using helium as the carrier gas at a flow rate of 1 ml min^{-1}. The GC oven temperature was held at 100°C for 3 min and increased to 300°C at 3.5° min^{-1} for a total run time of approximately 60 min. The MS source and quadrupole were held at 230°C and 150°C, respectively, and the detector was operated in selected ion monitoring (SIM) mode. MIDs were obtained for each measured metabolite and incorporated with extracellular flux measurements for flux determination. The identity and values of these measured fragments and fluxes are listed in Supplementary Table 1.

Flux estimation

Intracellular fluxes were estimated for a model reaction network by minimizing the lack of fit between actual and simulated flux and GC/MS measurements. The network contained simplified versions of glycolysis, the PPP, anaplerotic reactions, the TCA cycle, and amino acid biosynthesis. (The Supplement lists specific assumptions regarding the network and metabolism that were made for the sake of the flux analysis. Also see Supplementary Table 2 for a list of all network reactions and atom transitions.) We additionally calculated 95%

confidence intervals for each flux using parameter continuation (Antoniewicz et al., 2006). All flux simulation, estimation, and continuation in this study was conducted using Metran, a flux analysis tool built upon an EMU framework (Antoniewicz et al., 2007a, Yoo et al., 2008, Young et al., 2008). Some fluxes were virtually unidentifiable and approximate values were obtained from the literature (Hofmann et al., 2008, Munger et al., 2008).

Tracer evaluation

The effects of 18 ^{13}C-labeled tracers (11 glucose and 7 glutamine) on flux estimation precision were evaluated (see Table 1). Tracers were chosen if they were commercially available or if they had been previously cited in literature. The effectiveness of each tracer was gauged as follows:

1. A defined set of GC/MS and flux measurements was simulated for a given tracer (see Supplementary Table 3).

2. Standard errors of 5% for external flux measurements and 0.1–1 mol% for GC/MS MIDs were introduced randomly and normally.

3. Flux values and 95% confidence intervals were determined for each reaction.

The usefulness of a tracer was assumed to be directly linked to the precision with which it was able to estimate fluxes of interest; i.e., tracers producing narrower confidence intervals have greater value.

Precision scoring

To more easily compare estimate precision on a group basis, we created a precision scoring metric. Similar optimality criteria have been used previously for experimental design (Noh and Wiechert, 2006, Noh et al., 2006); however, these earlier methods have been based on the parameter covariance matrix, which assumes linearity and does not always truly capture the nonlinear, constrained systems studied in flux analysis. This precision scoring metric relies on the more robust and accurate nonlinear confidence intervals obtained via parameter continuation (Antoniewicz et al., 2006). First, a normalized range is calculated for each flux using the formula

$$r_i = \min\left(\frac{u_i}{|v_i|}, \frac{v_i}{|v_i|} + \alpha\right) - \max\left(\frac{l_i}{|v_i|}, \frac{v_i}{|v_i|} - \alpha\right)$$

(1)

where v_i, l_i, u_i, and r_i are the estimated flux, lower bound, upper bound, and normalized range for the ith flux, and α is a cut-off parameter that prevents one excessively distant bound from overly influencing the scoring. The individual ranges are next converted into scores using a negative exponential function and summed into a final overall score via the expression

$$S = \sum_i w_i \exp\left(-\frac{r_i}{\beta}\right)$$

(2)

where w_i is a weighting parameter for the ith flux, β is a range-scaling parameter, and S is the overall precision score. We empirically found that values of 1 and 3 for α and β result in a good dynamic range of scores. If each w_i can be simply zero or one (serving to either exclude or include fluxes in the overall score), each flux's precision score will range between zero (unidentifiable) and one (perfectly identifiable). The overall score will then range between zero and the number of fluxes under consideration.

Because the upper and lower bounds of any given confidence interval are sensitive to the random error introduced into the simulated measurements, the corresponding precision scores will also vary for simulated experiments with different random errors. To account for this, we conducted six simulated experiments for every tracer of interest and generated a distribution of precision scores, allowing us to report a mean precision score and a precision score standard deviation.

Results and Discussion

Experimental flux analysis

The metabolic phenotype of a cell is a key component of its overall behavior, and evidence suggests that metabolism plays an important role in maintaining the tumor phenotype (DeBerardinis et al., 2007). Metabolic analysis of cancer cells has again become an active area of research, and technological improvements have expanded our ability to investigate metabolism using stable isotopically labeled substrates. In this study we used the A549 cancer cell line as a model system for evaluating isotopic tracers in mammalian cells. This line is often used in molecular and metabolic studies of cancer and exhibits aerobic glycolysis, commonly known as the Warburg effect (Christofk et al., 2008, Hatzivassiliou et al., 2005). To obtain baseline values for our metabolic network we estimated fluxes of semi-confluent cells using an equimolar mixture of [U-^{13}C$_6$]glucose and [1-^{13}C]glucose, a combination of tracers commonly used in the literature (Noh et al., 2006, Sriram et al., 2008). The actual proportion of each tracer and naturally labeled glucose from serum was obtained from GC/MS measurements of extracellular glucose. Extracellular fluxes and MIDs of intracellular metabolites were used to estimate the flux distribution (see Supplementary Table 1 for all measurement data). The system possessed 101 redundant measurements and the expected upper bound of the 95% confidence region is 130, assuming that the minimized sum of squared residuals (SSR) followed a χ^2 distribution. Flux estimation resulted in a minimized SSR of 52, indicating that the fit was statistically acceptable. Estimated values and 95% confidence intervals for each independent flux are listed in Table 2. The overall metabolic network is depicted in Figure 1. Several exchange fluxes were difficult to precisely determine; in these cases, values were culled from literature.

As expected, the cancer cells displayed a high glycolytic flux and excreted most of the carbon as lactate. Approximately 15% of the glucose flux was diverted to the pentose phosphate shunt. However, these estimations did not include explicit measurements of pentose phosphate intermediates; as such, exchange fluxes within this pathway were unidentifiable (Table 2). TCA cycle fluxes were relatively low and largely driven by glutamine consumption. Interestingly, we observed a net flux toward citrate for the isocitrate dehydrogenase (IDH) reaction, indicating that this cell line undergoes reductive carboxylation of α-ketoglutarate (Figure 1). Finally, we estimated a significant flux from malate to pyruvate (malic enzyme) and a negligible flux through pyruvate carboxylase (pyruvate to oxaloacetate). Malic enzyme flux, which regenerates NADPH, can be assumed to compensate for the excessive NADPH requirements of fatty acid synthesis and any lost in the reductive carboxylation pathway (Deberardinis et al., 2008). Our results successfully described the metabolic phenotype of cancer cells and serve as a benchmark for our tracer analysis below.

Tracer confidence intervals

We next calculated confidence intervals for every combination of tracer and flux. Results for selected fluxes are shown in Figure 2, and the complete set of confidence intervals over all fluxes is available in Supplementary Figures 1 and 2.

Because the lower glycolytic fluxes consist primarily of stoichiometrically determined net fluxes and completely unidentifiable exchange fluxes, tracers of any kind offer no benefit in flux estimation and show little variation in confidence interval precision in this region of the network. Tracers do generate results of more diverse quality in upper glycolysis (see Figures 2A and 2B for examples). Here, glutamine tracers are completely ineffective, since there is no set of reactions by which any glutamine atom can travel to this portion of the network. Uniformly labeled glucose also gives nominal precision; because there are no other carbon sources feeding into glycolysis, all metabolites here are fully labeled by this tracer at isotopic steady state regardless of the flux distribution.

Glucose tracers labeled at some combination of the 4th, 5th, and 6th carbons give results of limited quality, primarily because these labeled atoms are trapped in a cycle. If M_i is the ith atom of metabolite M_i the atomic transitions show that glucose$_i$ (where $4 \leq i \leq 6$) will distribute ^{13}C to only $G6P_i$, $F6P_i$, $P5P_{i-1}$, $S7P_{i+1}$, $E4P_{i-2}$, GAP_{i-3}, and $DHAP_{i-3}$ before permanently exiting glycolysis and the PPP (see highlighted atom transitions for [4]Gluc in Figure 3B). This uniformity means that the key GC/MS fragment behind glycolysis flux estimation (GLP) will only be labeled at a single carbon, reducing the potential measurement diversity, which in turn reduces the sensitivity to fluxes. The 1st carbon of glucose feeds into a comparable positional carbon cycle, leading to [3-^{13}C]GLP and similarly decreased sensitivity. Tracers labeled at the 2nd or 3rd carbons ([1,2]Gluc, [2]Gluc, and [3]Gluc), however, capitalize on the atomic transitions of the subnetwork and distribute significant label to each carbon in GLP, producing the greatest sensitivity and most precise confidence intervals in glycolysis (see highlighted atom transitions for [2]Gluc in Figure 3A).

The estimation quality of the PPP closely reflects that of upper glycolysis. Instead of GLP, P5P is now the major contributing measurement. [U]Gluc and all glutamine tracers are again completely noninformative (for the same reasons as before). [4], [4,5], [5], and [6]Gluc are ineffective because label is once more restricted to a small subset of positions in the network. Because [1]Gluc loses its label to CO_2 in the oxidative PPP, P5P is predominantly unlabeled and demonstrates little sensitivity. Glucose labeled at the 2nd and 3rd positions are again the tracers that most confidently estimate fluxes. These behaviors are fairly consistent through all individual net and exchange fluxes of the PPP. Specific examples are shown in Figures 2D (transketolase net), 2E (transketolase exchange), and 2F (transaldolase exchange).

Glutamine tracers, on the other hand, generally provided better estimations of the pyruvate dehydrogenase flux, located at the junction between glycolysis and the TCA cycle (Figure 2C). Because both the 3rd and 4th carbons in glucose mostly transition to the 1st carbon of pyruvate and exit the system as CO_2 at this step, [3]Gluc, [3,4]Gluc, and [4]Gluc could not precisely resolve the PDH flux, despite their common use and effectiveness in previous experiments (Holleran et al., 1997, Munger et al., 2008). This discrepancy arises because these previous studies measured labeling in CO_2 while our analysis assumes no such measurement. Importantly, one cannot exchange measurement sets of MFA experiments and necessarily expect similar results or patterns when evaluating tracers.

While ^{13}C glutamine and uniformly labeled glucose tracers offered minimal information for glycolysis and the PPP, they demonstrated considerable utility in estimating TCA cycle and anaplerotic fluxes. Net fluxes within the TCA cycle (succinate to fumarate and oxaloacetate to fumarate) were best characterized when using glutamine tracers with two or more carbons, specifically [1,2]Gln, [3,4]Gln, and [U]Gln (Figure 2G and Figure 2H). Because the glutamine flux into the TCA cycle is significantly smaller than the incoming glucose flux, multiply labeled glutamine tracers are presumably more useful because they introduce

greater amounts label that are less easily diluted (see Figures 3C and 3D to compare atom transitions for [3,4]Gln and [4]Gln). The effectiveness of these tracers was further highlighted by the improved confidence intervals obtained for exchange fluxes in the TCA cycle and malic enzyme reactions (Figures 2I–2L). Exchange between succinate, fumarate, and oxaloacetate are key reactions within oxidative metabolism that also affect cofactor levels and pyruvate cycling; therefore, precise estimation of these reactions are of paramount importance for cancer research (Hatzivassiliou et al., 2005, Deberardinis et al., 2008).

To better describe the quality of data and simulations obtained from specific tracers, we calculated precision scores for each tracer, covering both subnetworks and central carbon metabolism in its entirety. Independent fluxes included in the scoring for each subnetwork are described in Supplementary Figure 3. All glucose tracers except [U]Gluc scored well for glycolysis, with [1,2]Gluc, [2]Gluc, and [3]Gluc performing significantly better than most (Figure 4A). These three tracers provided the best scores (i.e., the most precise estimates) for the PPP as well (Figure 4B). The highest scoring glucose tracer for TCA cycle analysis was [U]Gluc (Figure 4C). Three glutamine tracers also generated similarly high scores and precise estimates within the TCA cycle subnetwork; in particular, those tracers labeled at two or more positions scored best ([1,2]Gln, [3,4]Gln, and [U]Gln). Finally, the best overall tracer for analyzing the entire cancer cell flux network was [1,2]Gluc, followed by other glucose tracers labeled at the 2nd or 3rd carbons (Figure 4D). Although these tracers did not generate the best results for the TCA cycle, their unique ability to consistently characterize fluxes throughout the entire network resulted in superior scores compared to other tracers.

Conclusion

The metabolic phenotype of tumors has reemerged as an important area of study and potential clinical target (Kroemer and Pouyssegur, 2008). Fueled by advanced computational software and technologies, researchers can now characterize cellular metabolism in unprecedented detail. To better demonstrate the utility of isotopic tracers for cancer research, we have quantitatively and comparatively described the precision of uniquely labeled ^{13}C glucose and glutamine tracers for flux determination in mammalian cells. An EMU-based algorithm enabled the high-throughput flux estimations and confidence interval calculations required for this description. Table 3 summarizes the optimal tracers to use for estimating each flux, specific subnetworks, and central carbon metabolism as a whole. [1,2]Gluc provided the highest level of precision for the overall network, glycolysis, and the PPP, while [U]Gluc and multiply labeled glutamine tracers were most informative for the TCA cycle. Specific instances of their use are present in the literature (Boros et al., 2005, Munger et al., 2008, Yoo et al., 2008); however, we hope the demonstrable improvements of precision described here help to propagate the use of more effective tracer molecules in future MFA experiments.

The tracer evaluation process and accompanying results in this study provide a general procedure for the experimental design of isotopic tracer studies. However, it should be noted that specific cell types exhibit particular flux profiles, which in turn will affect the results generated by simulated tracer studies such as those presented here. As such, our findings are network dependent and therefore most relevant to the study of tumor cells. Furthermore, the precision of our flux estimations are dependent upon the metabolites measured. As mass spectrometry and other related technologies continue to improve, researchers will obtain richer data sets to incorporate into the estimation process (Munger et al., 2008, Hofmann et al., 2008). Nevertheless, our results should be valid for most mammalian systems given the conserved nature of atom transitions in central carbon metabolism. In cells with significantly different networks and/or flux distributions (e.g., gluconeogenic hepatocytes) these specific tracer simulations may not apply (Yang et al., 2008). However, our methodology will still

prove useful in optimizing experimental design, especially in complex systems where the best tracer cannot be determined *a priori*. Future studies requiring more rigorous simulations will aim to identify combinations of differentially labeled substrates that can further improve the precision of flux estimations. In the meantime, these results can serve as a guide for systems biologists to more effectively design experiments to study metabolism at a global level.

Supplementary Material

Refer to Web version on PubMed Central for supplementary material.

Acknowledgments

Nomenclature

3PG	3-phosphoglycerate
6PG	6-phosphogluconate
AcCoA	acetyl coenzyme A
AKG	α-ketoglutarate
Ala	alanine
Asp	aspartate
Cit	citrate
Cyt	cytosolic
DHAP	dihydroxyacetone phosphate
E4P	erythrose 4-phosphate
Ext	extracellular
F6P	fructose 6-phosphate
FA	fatty acids
Fum	fumarate
G6P	glucose 6-phosphate
GAP	glyceraldehyde 3-phosphate
Gln	glutamine
GLP	glycerol 3-phosphate
Glu	glutamate
Gluc	glucose
Gly	glycine
Lac	lactate
Mal	malate

Mit	mitochondrial
NTP	nucleotide tri-phosphate
OAA	oxaloacetate
P5P	pentose 5-phosphate
Pyr	pyruvate
S7P	seduheptulose 7-phosphate
Ser	serine
Suc	succinate

References

Antoniewicz MR, Kelleher JK, Stephanopoulos G. Determination of confidence intervals of metabolic fluxes estimated from stable isotope measurements. Metab Eng 2006;8:324–337. [PubMed: 16631402]

Antoniewicz MR, Kelleher JK, Stephanopoulos G. Elementary metabolite units (EMU): a novel framework for modeling isotopic distributions. Metab Eng 2007a;9:68–86. [PubMed: 17088092]

Antoniewicz MR, Kraynie DF, Laffend LA, Gonzalez-Lergier J, Kelleher JK, Stephanopoulos G. Metabolic flux analysis in a nonstationary system: fed-batch fermentation of a high yielding strain of E. coli producing 1,3-propanediol. Metab Eng 2007b;9:277–292. [PubMed: 17400499]

Borner J, Buchinger S, Schomburg D. A high-throughput method for microbial metabolome analysis using gas chromatography/mass spectrometry. Anal Biochem 2007;367:143–151. [PubMed: 17585867]

Boros LG, Lerner MR, Morgan DL, Taylor SL, Smith BJ, Postier RG, Brackett DJ. [1,2-13C2]-D-glucose profiles of the serum, liver, pancreas, and DMBA-induced pancreatic tumors of rats. Pancreas 2005;31:337–343. [PubMed: 16258367]

Boros LG, Steinkamp MP, Fleming JC, Lee WN, Cascante M, Neufeld EJ. Defective RNA ribose synthesis in fibroblasts from patients with thiamine-responsive megaloblastic anemia (TRMA). Blood 2003;102:3556–3561. [PubMed: 12893755]

Burgess SC, He T, Yan Z, Lindner J, Sherry AD, Malloy CR, Browning JD, Magnuson MA. Cytosolic phosphoenolpyruvate carboxykinase does not solely control the rate of hepatic gluconeogenesis in the intact mouse liver. Cell Metab 2007;5:313–320. [PubMed: 17403375]

Chang Y, Suthers PF, Maranas CD. Identification of optimal measurement sets for complete flux elucidation in metabolic flux analysis experiments. Biotechnol Bioeng 2008;100:1039–1049. [PubMed: 18553391]

Christofk HR, Vander Heiden MG, Harris MH, Ramanathan A, Gerszten RE, Wei R, Fleming MD, Schreiber SL, Cantley LC. The M2 splice isoform of pyruvate kinase is important for cancer metabolism and tumour growth. Nature 2008;452:230–233. [PubMed: 18337823]

Deberardinis RJ, Mancuso A, Daikhin E, Nissim I, Yudkoff M, Wehrli S, Thompson CB. Beyond aerobic glycolysis: transformed cells can engage in glutamine metabolism that exceeds the requirement for protein and nucleotide synthesis. Proc Natl Acad Sci U S A 2007;104:19345–19350. [PubMed: 18032601]

Deberardinis RJ, Sayed N, Ditsworth D, Thompson CB. Brick by brick: metabolism and tumor cell growth. Curr Opin Genet Dev 2008;18:54–61. [PubMed: 18387799]

Hatzivassiliou G, Zhao F, Bauer DE, Andreadis C, Shaw AN, Dhanak D, Hingorani SR, Tuveson DA, Thompson CB. ATP citrate lyase inhibition can suppress tumor cell growth. Cancer Cell 2005;8:311–321. [PubMed: 16226706]

Hellerstein MK. New stable isotope-mass spectrometric techniques for measuring fluxes through intact metabolic pathways in mammalian systems: introduction of moving pictures into functional genomics and biochemical phenotyping. Metab Eng 2004;6:85–100. [PubMed: 14734258]

Hofmann U, Maier K, Niebel A, Vacun G, Reuss M, Mauch K. Identification of metabolic fluxes in hepatic cells from transient 13C-labeling experiments: Part I. Experimental observations. Biotechnol Bioeng 2008;100:344–354. [PubMed: 18095337]

Holleran AL, Fiskum G, Kelleher JK. Quantitative analysis of acetoacetate metabolism in AS-30D hepatoma cells with 13C and 14C isotopic techniques. Am J Physiol 1997;272:E945–E951. [PubMed: 9227436]

Kharroubi AT, Masterson TM, Aldaghlas TA, Kennedy KA, Kelleher JK. Isotopomer spectral analysis of triglyceride fatty acid synthesis in 3T3-L1 cells. Am J Physiol 1992;263:E667–E675. [PubMed: 1415685]

Kleijn RJ, Geertman JM, Nfor BK, Ras C, Schipper D, Pronk JT, Heijnen JJ, Van Maris AJ, Van Winden WA. Metabolic flux analysis of a glycerol-overproducing Saccharomyces cerevisiae strain based on GC-MS, LC-MS and NMR-derived C-labelling data. FEMS Yeast Res 2007;7:216–231. [PubMed: 17132142]

Kroemer G, Pouyssegur J. Tumor cell metabolism: cancer's Achilles' heel. Cancer Cell 2008;13:472–482. [PubMed: 18538731]

Munger J, Bennett BD, Parikh A, Feng XJ, Mcardle J, Rabitz HA, Shenk T, Rabinowitz JD. Systems-level metabolic flux profiling identifies fatty acid synthesis as a target for antiviral therapy. Nat Biotechnol. 2008

Neese RA, Faix D, Kletke C, Wu K, Wang AC, Shackleton CH, Hellerstein MK. Measurement of endogenous synthesis of plasma cholesterol in rats and humans using MIDA. Am J Physiol 1993;264:E136–E147. [PubMed: 8430782]

Nielsen J. It is all about metabolic fluxes. J Bacteriol 2003;185:7031–7035. [PubMed: 14645261]

Noh K, Wahl A, Wiechert W. Computational tools for isotopically instationary 13C labeling experiments under metabolic steady state conditions. Metab Eng 2006;8:554–577. [PubMed: 16890470]

Noh K, Wiechert W. Experimental design principles for isotopically instationary 13C labeling experiments. Biotechnol Bioeng 2006;94:234–251. [PubMed: 16598793]

Rantanen A, Mielikainen T, Rousu J, Maaheimo H, Ukkonen E. Planning optimal measurements of isotopomer distributions for estimation of metabolic fluxes. Bioinformatics 2006;22:1198–1206. [PubMed: 16504982]

Sauer U. Metabolic networks in motion: 13C-based flux analysis. Mol Syst Biol 2006;2:62. [PubMed: 17102807]

Sekhon BK, Roubin RH, Tan A, Chan WK, Sze DM. High-throughput screening platform for anticancer therapeutic drug cytotoxicity. Assay Drug Dev Technol 2008;6:711–721. [PubMed: 19035851]

Sriram G, Rahib L, He JS, Campos AE, Parr LS, Liao JC, Dipple KM. Global metabolic effects of glycerol kinase overexpression in rat hepatoma cells. Mol Genet Metab 2008;93:145–159. [PubMed: 18029214]

Stephanopoulos G, Vallino JJ. Network rigidity and metabolic engineering in metabolite overproduction. Science 1991;252:1675–1681. [PubMed: 1904627]

Tang YJ, Martin HG, Dehal PS, Deutschbauer A, Llora X, Meadows A, Arkin A, Keasling JD. Metabolic flux analysis of Shewanella spp. reveals evolutionary robustness in central carbon metabolism. Biotechnol Bioeng 2009a;102:1161–1169. [PubMed: 19031428]

Tang YJ, Martin HG, Myers S, Rodriguez S, Baidoo EE, Keasling JD. Advances in analysis of microbial metabolic fluxes via (13)C isotopic labeling. Mass Spectrom Rev 2009b;28:362–375. [PubMed: 19025966]

Yang L, Kasumov T, Kombu RS, Zhu SH, Cendrowski AV, David F, Anderson VE, Kelleher JK, Brunengraber H. Metabolomic and mass isotopomer analysis of liver gluconeogenesis and citric acid cycle: II. Heterogeneity of metabolite labeling pattern. J Biol Chem 2008;283:21988–21996. [PubMed: 18544526]

Yoo H, Antoniewicz MR, Stephanopoulos G, Kelleher JK. Quantifying reductive carboxylation flux of glutamine to lipid in a brown adipocyte cell line. J Biol Chem 2008;283:20621–20627. [PubMed: 18364355]

Young JD, Walther JL, Antoniewicz MR, Yoo H, Stephanopoulos G. An elementary metabolite unit (EMU) based method of isotopically nonstationary flux analysis. Biotechnol Bioeng 2008;99:686–699. [PubMed: 17787013]
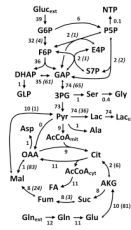
Figure 1.
Experimentally determined fluxes representing central carbon metabolism in tumor cells. Extracellular fluxes and MIDs were measured and incorporated into the network shown (see Supplementary Table 2). An acceptable fit was obtained with a sum of squared residuals (SSR) of 52, well under the upper bound of the 95% confidence region for a χ^2 distribution. Net fluxes are listed first for each reaction and exchange fluxes are within parenthesis. Units for all fluxes are nmol min^{-1} mg $protein^{-1}$. Italicized numbers represent flux values that were taken from literature since they were unidentifiable for our particular experiment.
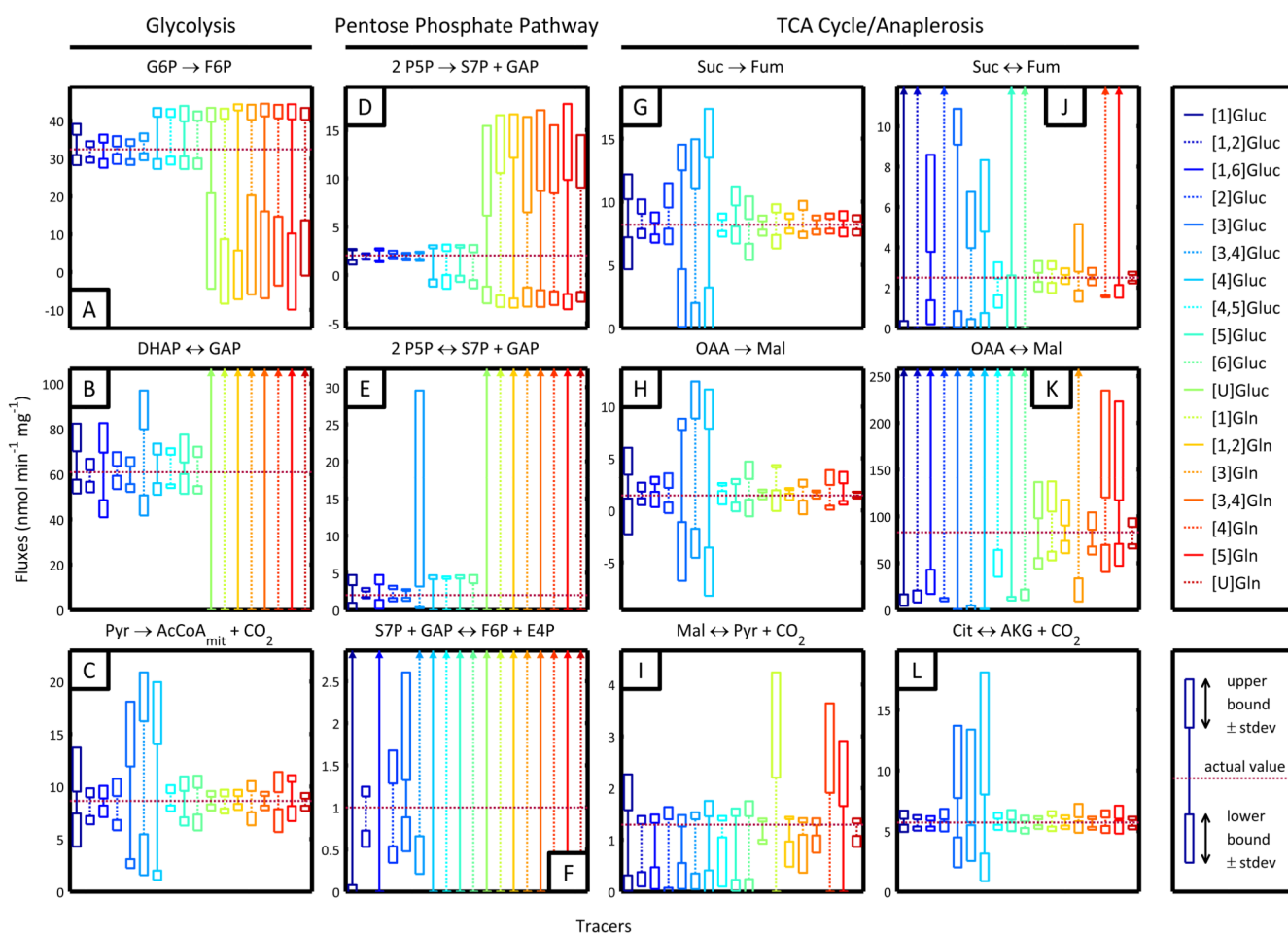
Figure 2.
Simulated confidence intervals for selected fluxes when using specific isotopic tracers. Horizontal dashed lines indicate actual fluxes. Upper and lower bounds of the 95% confidence interval are illustrated for each simulated tracer. The standard error of both upper and lower bounds is represented by the boxes at the top and bottom of each interval. (A) Glucose-6-phosphate isomerase and (B) triose-phosphate isomerase fluxes demonstrate the effectiveness of glucose tracers in estimated glycolytic fluxes. (C) Pyruvate dehydrogenase flux is most precisely estimated by most glutamine tracers and some glucose tracers. (D–F) Net and exchange fluxes within the pentose phosphate pathway are best determined with glucose tracers labeled at the 1st, 2nd, or 3rd carbon, with [1,2]glucose performing best. (G,H) Net fluxes and (I–L) exchange fluxes in the TCA cycle are characterized well using [U]Gluc, [1,2]Gln, [3,4]Gln, or [U]Gln.
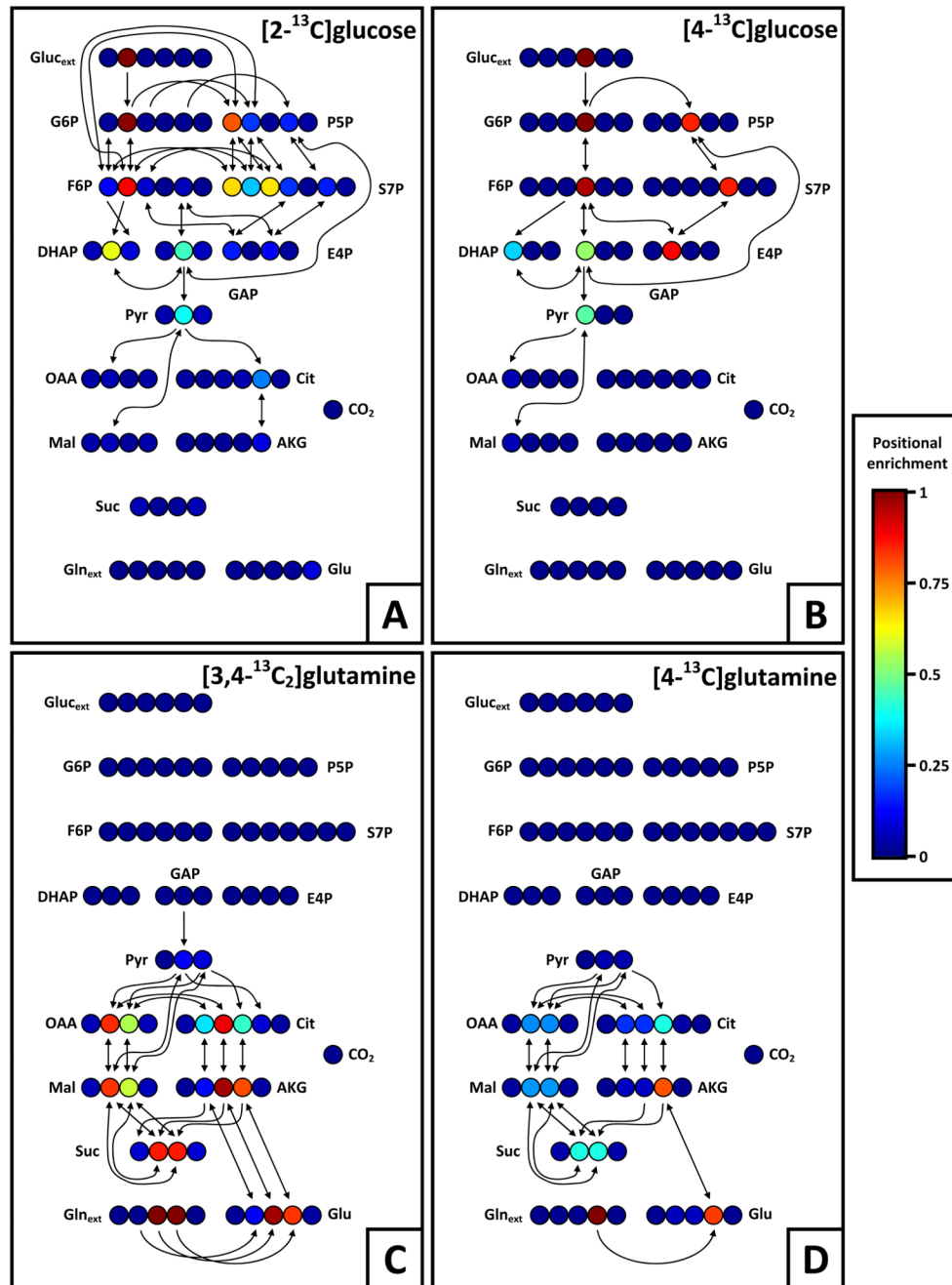
Figure 3.
Atom transition networks and positional fractional labeling for selected glucose and glutamine tracers. Fractional labeling is indicated by a colormap, where dark red indicates all atoms at that position are ^{13}C and dark blue that all atoms are ^{12}C. No natural labeling was assumed in the creation of these maps. Atom transitions are indicated for all positions where fractional ^{13}C labeling exceeds 10%. (A) [2]Gluc effectively characterizes glycolytic and PPP fluxes because DHAP (and by extension GLP) is labeled in multiple positions by different combinations of fluxes, leading to greater measurement sensitivity. (B) [4]Gluc poorly identifies fluxes in glycolysis and the PPP because its sole labeled carbon is caught in a cycle and can only reach the 1st carbon of DHAP. (C and D) [3,4]Gln and [4]Gln are both

able to label a majority of the carbon atoms in the TCA cycle; however, the two labeled atoms in the former lead to larger, clearer measurements and therefore more precises fluxes.
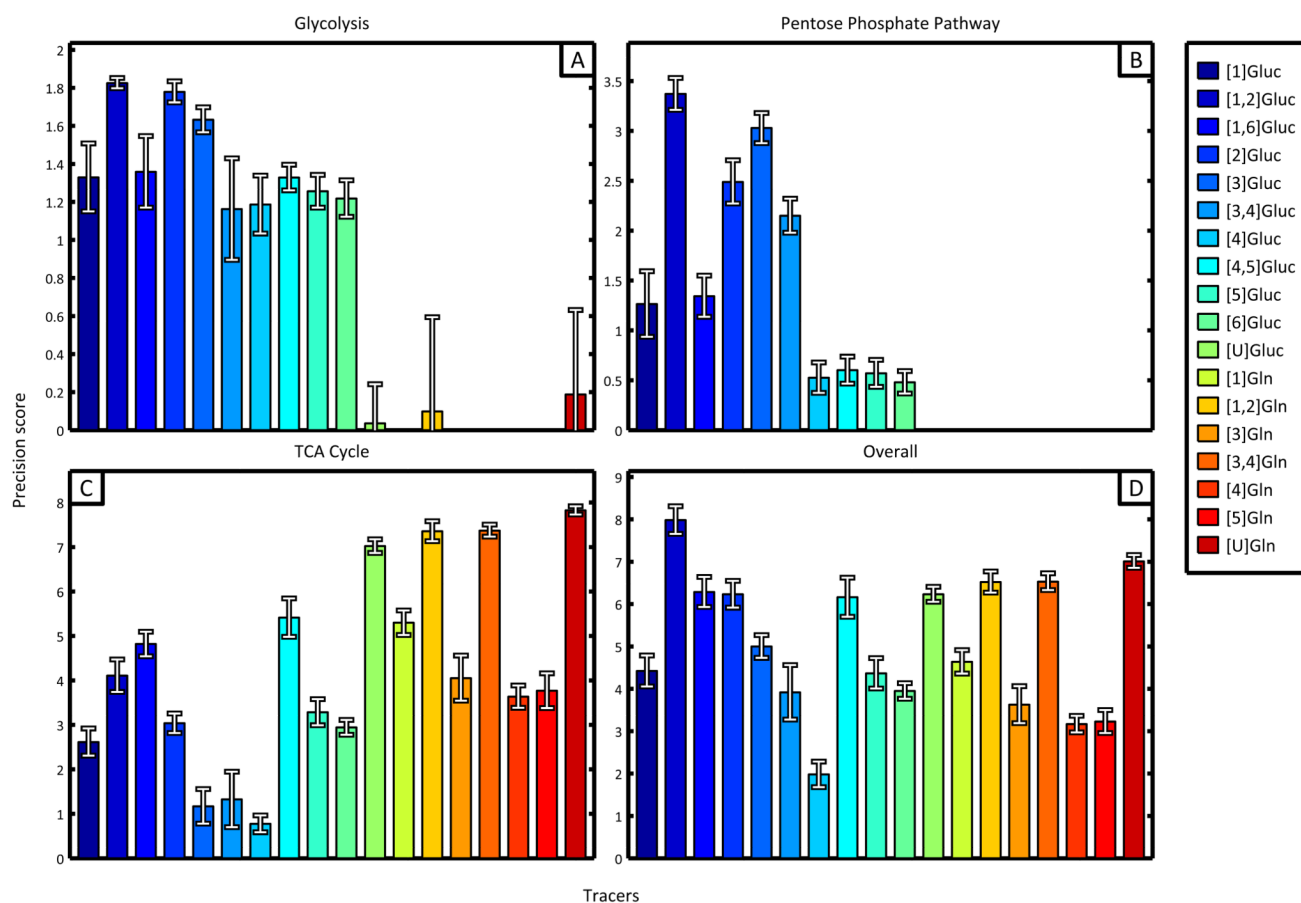
Figure 4.
Results obtained from precision scoring algorithm identify the optimal tracer for analysis of subnetworks and central carbon metabolism. The precision scores resulting from simulated experiments involving only natural labeling have been subtracted from each displayed tracer score to aid in visual differentiation and comparison. (A) Glycolysis and (B) pentose phosphate subnetworks are best described by [1,2]Gluc, [2]Gluc, and [3]Gluc. (C) TCA cycle scores were highest for [U]glucose and several glutamine tracers labeled at two or more carbons. (D) The most precise tracer for analysis of the entire network was [1,2]Gluc.

Table 1

Glucose and glutamine tracers

Tracer	Abbreviation
[1-^{13}C]glucose	[1]Gluc
[1,2-^{13}C$_2$]glucose	[1,2]Gluc
[1,6-^{13}C$_2$]glucose	[1,6]Gluc
[2-^{13}C]glucose	[2]Gluc
[3-^{13}C]glucose	[3]Gluc
[3,4-^{13}C$_2$]glucose	[3,4]Gluc
[4-^{13}C]glucose	[4]Gluc
[4,5-^{13}C$_2$]glucose	[4,5]Gluc
[5-^{13}C]glucose	[5]Gluc
[6-^{13}C]glucose	[6]Gluc
[U-^{13}C$_6$]glucose	[U]Gluc
[1-^{13}C]glutamine	[1]Gln
[1,2-^{13}C$_2$]glutamine	[1,2]Gln
[3-^{13}C]glutamine	[3]Gln
[3,4-^{13}C$_2$]glutamine	[3,4]Gln
[4-^{13}C]glutamine	[4]Gln
[5-^{13}C]glutamine	[5]Gln
[U-^{13}C$_6$]glutamine	[U]Gln

Table 2

Experimentally determined net ($\rightarrow$) and exchange ($\leftrightarrow$) fluxes and 95% flux confidence intervals for the A549 carcinoma cell

Glycolysis

Reaction	Flux	Interval
$Gluc_{ext} \rightarrow G6P$	38.6	[34.7, 43.2]
$G6P \rightarrow F6P$	32.4	[29.7, 35.1]
$G6P \leftrightarrow F6P$	0.0	[0.0, Inf]
$F6P \rightarrow DHAP + GAP$	36.5	[32.6, 40.7]
$DHAP \rightarrow GAP$	35.5	[31.6, 39.7]
$DHAP \leftrightarrow GAP$	0.0	[0.0, 258.7]
$GAP \rightarrow 3PG$	74.0	[65.7, 82.8]
$GAP \leftrightarrow 3PG$	0.0	[0.0, Inf]
$3PG \rightarrow Pyr$	73.1	[64.8, 81.9]
$Pyr \rightarrow Lac$	73.6	[65.8, 83.3]
$Pyr \leftrightarrow Lac$	13420	[0.0, Inf]
$Lac \rightarrow Lac.x$	73.6	[65.8, 83.3]

Pentose Phosphate Pathway

Reaction	Flux	Interval
$G6P \rightarrow 6PG$	6.2	[5.4, 7.4]
$6PG \rightarrow P5P + CO2$	6.2	[5.4, 7.4]
$2\ P5P \rightarrow S7P + GAP$	2.0	[1.8, 2.4]
$2\ P5P \leftrightarrow S7P + GAP$	19290	[0.0, Inf]
$S7P + GAP \rightarrow F6P + E4P$	2.0	[1.8, 2.4]
$S7P + GAP \leftrightarrow F6P + E4P$	0.0	[0.0, 0.4]
$P5P + E4P \rightarrow F6P + GAP$	2.0	[1.8, 2.4]
$P5P + E4P \leftrightarrow F6P + GAP$	0.0	[0.0, 0.6]

TCA Cycle/Anaplerosis

Reaction	Flux	Interval
$Pyr + CO2 \rightarrow OAA$	0.0	[0.0, 1.7]
$Mal \rightarrow Pyr + CO2$	9.6	[8.5, 10.7]
$Mal \leftrightarrow Pyr + CO2$	1.3	[0.9, 1.6]
$Pyr \rightarrow AcCoA_{mit} + CO2$	8.6	[5.5, 11.0]
$AcCoA_{mit} + OAA \rightarrow Cit$	8.6	[5.5, 11.0]
$AKG + CO_2 \rightarrow Cit$	2.0	[0.2, 3.6]
$AKG + CO_2 \leftrightarrow Cit$	5.7	[4.6, 7.1]
$AKG \rightarrow Suc + CO2$	8.2	[6.6, 10.7]
$Suc \rightarrow Fum$	8.2	[6.6, 10.7]

TCA Cycle/Anaplerosis

Reaction	Flux	Interval
Suc ↔ Fum	0.2	[0.0, Inf]
Fum → Mal	8.2	[6.6, 10.7]
Fum ↔ Mal	23.8	[5.2, Inf]
OAA → Mal	1.4	[0.8, 2.9]
OAA ↔ Mal	106200	[35.9, Inf]

Amino Acid Metabolism

Reaction	Flux	Interval
Gln_{ext} → Gln	11.5	[10.4, 12.6]
Gln → Glu	11.0	[9.9, 12.1]
Glu → AKG	8.2	[7.0, 9.3]
Glu ↔ AKG	81.3	[35.9, 480.3]
Pyr + Glu → Ala + AKG	0.5	[0.4, 0.6]
OAA + Glu → Asp + AKG	0.6	[0.5, 0.7]
3PG + Glu → Ser + AKG	0.9	[0.8, 1.1]
Ser → Gly + MEETHF	0.4	[0.3, 0.4]

Biomass Formation

Reaction	Flux	Interval
P5P → NTP	0.1	[0.1, 0.1]
DHAP → GLP	1.0	[0.8, 1.2]
Cit → $AcCoA_{cyt}$ + OAA	10.7	[5.3, 14.5]
$AcCoA_{cyt}$ → FA	10.7	[5.3, 14.5]
Amino acids → Biomass	3.3	[2.7, 4.0]

Table 3

Optimal tracers for net (→) and exchange (↔) fluxes for the A549 carcinoma cell

Glycolysis

Reaction	Best Tracer(s)
$Gluc_{ext} \to G6P$	[1,2] & [2]Gluc
$G6P \to F6P$	[1,2]Gluc
$G6P \leftrightarrow F6P$	[3] & [3,4]Gluc
$F6P \to DHAP + GAP$	[1,2] & [2]Gluc
$DHAP \to GAP$	[1,2]Gluc
$DHAP \leftrightarrow GAP$	[1,2]Gluc
$GAP \to 3PG$	[1,2] & [2]Gluc
$GAP \leftrightarrow 3PG$	none
$3PG \to Pyr$	[1,2]Gluc
$Pyr \to Lac$	[1,2] & [2]Gluc
$Pyr \leftrightarrow Lac$	none
$Lac \to Lac.x$	[1,2] & [2]Gluc

Pentose Phosphate Pathway

Reaction	Best Tracer(s)
$G6P \to 6PG$	[1,2]Gluc
$6PG \to P5P + CO2$	[1,2]Gluc
$2 P5P \to S7P + GAP$	[1,2] & [3]Gluc
$2 P5P \leftrightarrow S7P + GAP$	[1,2]Gluc
$S7P + GAP \to F6P + E4P$	[1,2]& [3]Gluc
$S7P + GAP \leftrightarrow F6P + E4P$	[1,2]Gluc
$P5P + E4P \to F6P + GAP$	[1,2] & [3]Gluc
$P5P + E4P \leftrightarrow F6P + GAP$	[1,2] & [3]Gluc

TCA Cycle/Anaplerosis

Reaction	Best Tracer(s)
$Pyr + CO2 \to OAA$	[U]Gln
$Mal \to Pyr + CO2$	[U] & [3,4]Gln
$Mal \leftrightarrow Pyr + CO2$	[U]Gln
$Pyr \to AcCoA_{mit} + CO2$	[U]Gln
$AcCoA_{mit} + OAA \to Cit$	[U]Gln
$AKG + CO_2 \to Cit$	[U], [1,2] & [3,4]Gln
$AKG + CO_2 \leftrightarrow Cit$	[U]Gln
$AKG \to Suc + CO2$	[U] & [3,4]Gln
$Suc \to Fum$	[U] & [3,4]Gln
$Suc \leftrightarrow Fum$	[U] & [1,2]Gln

TCA Cycle/Anaplerosis

Reaction	Best Tracer(s)
Fum → Mal	[U] & [3,4]Gln
Fum ↔ Mal	[U]Gln
OAA → Mal	[U]Gln
OAA ↔ Mal	[U]Gln

Amino Acid Metabolism

Reaction	Best Tracer(s)
Gln_{ext} → Gln	[3], [U] & [3,4]Gln
Gln → Glu	[3], [U] & [3,4]Gln
Glu → AKG	[3], [U] & [3,4]Gln
Glu ↔ AKG	[U]Gln